# Gas adsorption in the inside and outside of single-walled carbon nanotubes

Akihiko Fujiwara [a,1] Kenji Ishii [a] Hiroyoshi Suematsu [a]
Hiromichi Kataura [b] Yutaka Maniwa [b] Shinzou Suzuki [c]
Yohji Achiba [c]

[a] *Department of Physics, School of Science, University of Tokyo, 7-3-1 Hongo, Bunkyo-ku, Tokyo 113-0033, Japan*

[b] *Department of Physics, School of Science, Tokyo Metropolitan University, 1-1 Minami-osawa, Hachi-oji, Tokyo 192-0397, Japan*

[c] *Department of Chemistry, School of Science, Tokyo Metropolitan University, 1-1 Minami-osawa, Hachi-oji, Tokyo 192-0397, Japan*

**Abstract**

Adsorption properties of nitrogen and oxygen gases in single-walled carbon nanotube bundles were investigated by the isotherm and x-ray diffraction studies. In the as-grown nanotubes with close-ended caps, both the gases are adsorbed only in the interstitial channels between triangular packed nanotubes. In the heat-treated nanotubes with open ends, the gases are adsorbed first in the inside of tubes, and next in the interstitial channels. In each site, gases can be adsorbed with the stoichiometory of $C_{20}N_2$ or $C_{20}O_2$ as a monolayer. These results indicate that the inside of nanotube has strong affinity for gas adsorption than the interstitial channels of bundles.

*Key words:* Carbon nanotubes, Gas adsorption, Structure

[1] Corresponding author. Tel.: +81-3-5841-4129; Fax: +81-3-5841-4532; E-mail address: fujiwara@phys.s.u-tokyo.ac.jp.

## 1 INTRODUCTION

Since the discovery of carbon nanotubes[1], it has attracted great attention to novel structural and electronic properties because of the one-dimensional structure and the tubular honeycomb-network in the nanometer scale. In a viewpoint of structural properties, carbon nanotubes have inner hollow cavity with diameters typically between 1 and 20 nanometers, and can be filled by certain substances[2,3]. This leads to interesting possible applications, such as gas absorbent [4,5] and molds to form the one dimensional (quantum) system[6]. For the gas adsorption, there are two different adsorption sites in a single-walled carbon nanotube (SWNT) bundle, namely, the inside of SWNTs (site A) and the interstitial channels of the bundle (site B) as shown in Fig. 1. From this figure, we can expect high gas-storage capacity in the SWNT bundle. Actually, high performance in hydrogen storage in SWNTs were reported [4]. Very recently, Maniwa *et al.*[7,8] reported that the change in the x-ray diffraction (XRD) profile for heat-treated (HT) SWNTs can be understood by gas adsorption in the site A. It is known that the heat-treatment in the presence of oxygen ($O_2$) or carbon dioxide ($CO_2$) results in opening caps at ends of nanotubes[2,9]. Therefore, it is suggested that HT-SWNTs have open-ended structure and can accept substances inside, while as-grown (AG) SWNTs have close-ended structure. Up to now, the gas-storage properties and the positions of stored gases are not clarified in detail, though it is very interesting in fundamental and will give an important information to the application of SWNTs to gas-storage materials. In this paper, we present gas (nitrogen ($N_2$) and $O_2$) adsorption properties of SWNT bundles. XRD studies during the adsorption processes were also performed in order to determine the position of gas. We find that AG-SWNTs adsorb gases in the interstitial channels between nanotubes in the bundle, whereas gases are adsorbed mostly on the inside surface of nanotubes firstly and next they are adsorbed in the interstitial channels for HT-SWNTs.

## 2 EXPERIMENTAL

The samples of SWNT bundles were synthesized by evaporation of composite rods of nickel (Ni), yttrium (Y) and graphite in helium atmosphere by arc discharge [10,11]. Observations by transmission electron microscopy (TEM) revealed that the soots contain a large quantity of SWNTs and also amorphous carbons and metal particles. It is also confirmed that SWNTs form hexagonal lattice; the diameter of bundle $D$ was typically 5 - 20 nm. The radius of tube $R_t$ used here is determined as about $0.7 \pm 0.1$ nm by Raman frequency of a breathing mode and TEM observation. We performed experiments on two kinds of samples as adsorbents, the AG-SWNTs with close-ended structure

and the HT-SWNTs (heat-treated in air at 350 °C for an hour) with open-ended structure.

Adsorption experiments for isotherm were done by the conventional volumetric method on samples of 15 - 25 mg amount. XRD measurements were performed in a transmission powder diffraction configuration by using CuK$\alpha$ radiation ($\lambda$ = 1.54Å). We used an imaging plate (IP) for detection. The spectrum (wave-vector transfer $Q$ vs. intensity) was obtained by integrating the intensity of Debye-Sherrer rings along the rings with a certain bandwidth. All measurements were performed at 77.3 K. The saturation pressure $p_0$ for $N_2$ and $O_2$ at this temperature is 760 and 156 Torr, respectively. The details of experimental methods and technics have been described elsewhere [12–14].

## 3 RESULTS AND DISCUSSION

Figure 2 shows adsorption isotherms of $N_2$ and $O_2$ on AG- and HT-SWNT samples, where the $V$ is defined as the gas volume per gross weight of sample. With increasing specific pressure $p/p_0$, the volume of adsorbed gas steeply increases below $p/p_0 \approx 0.01$ and moderately increases until $p/p_0 \approx 0.8$ followed by a steep increase. This is common feature for AG- and HT-SWNTs and for $N_2$ and $O_2$ gases. By applying Brunauer-Emmett-Teller (BET) method[15] to data in Fig. 2, we obtain monolayer adsorption capacity $V_m$ and specific surface area for adsorption $A_s$, where the molecular cross-section areas of 0.162 and 0.136 nm$^2$ are used for $N_2$ and $O_2$ molecule, respectively[16]; results are summarized in Table I. We find two clear features in adsorption properties. One is that $A_s$ of HT-SWNTs is about twice that of AG-SWNTs for both cases of $N_2$- and $O_2$-adsorption. This result suggests that the heat-treatment provides another adsorption site in addition to that of AG-SWNTs. Though the result for the $N_2$ adsorption in AG-SWNTs is similar to that reported by Stepanek *et al.*[17], that for SWNTs with "open" ends is the contrary; $V_m$ and $A_s$ are reduced by chemical opening in ref. [17], which is claimed to be due not to the "opening" effect but to the external effect, such as the agglomeration of SWNTs and the filling the inside of SWNTs by acid[17]. The adsorption site will be discussed later in detail. The other is the adsorbate dependence of $A_s$. $A_s$ for $O_2$-adsorption is larger than that for $N_2$-adsorption by about 6.6 % in greater detail in both cases of AG- and HT-SWNTs. This might be attributed to the use of general value for the cross section of molecules, which is not almighty[16].

We focus on the gas adsorption site for $V$ up to arround $V_m$, namely , monolayer adsorption. Figure 3 shows the dependence of the x-ray diffraction pattern on $O_2$ pressure for (a) AG- and (b) HT-SWNTs. As the *10* reflection peak is superposed on a large background increasing at low $Q$ as shown in the insets

of Fig. 3, the profile analyses was made after subtraction of the background as shown in Fig. 3: the index is referred to the two-dimensional hexagonal lattice of SWNTs [18]. The relative peak intensity $I/I_0$ and the position $Q_{10}$ of *10* reflection for all samples are plotted as a function of the adsorbed gas volume $V$ in Figs. 4(a) and 4(b), where $V$ is determined from the isotherm (Fig. 2) and the specific pressure in the XRD measurement. In AG-SWNTs, with increasing $V$ the $I/I_0$ increases and $Q_{10}$ shifts toward lower $Q$. On the other hand, in HT-SWNTs $I/I_0$ decreases monotonically but $Q_{10}$ does not shift up to $V \approx 70$ cm$^3$(stp)/g, and $I/I_0$ gradually decreases with the peak shift to lower $Q$.

We now examine structural models which account for the variation of intensity and position of *10* reflection through the gas adsorption. It is known that the peak intensity and position of the *10* reflection is very sensitive not only to the scattering factor and the lattice constant of the bundles but also to many other parameters, *i.e.*, radius of nanotube $R_{\rm t}$, size of the bundle (coherence length of hexagonal lattice) $D$ and their distribution[19,20]. However, we can expect that $R_{\rm t}$, $D$ and their distribution do not change during experiments because XRD measurements in each series were performed on the same sample under low gas pressure. Thus we can discuss the structural model where only three parameters are taken into account; lattice constant $a$, amount of the adsorbed gas molecules per carbon atom in the site A ($n_{\rm IN}$) and B ($n_{\rm OUT}$). In this assumption, the profile functions of *10* reflection can be obtained as follows:

$$
\begin{aligned}
& I(Q, a, n_{\rm IN}, n_{\rm OUT}) \\
&= \left| \sum_{n={\rm C,g}} f_n(Q) e^{2\pi i(h\cdot u_n + k\cdot v_n + l\cdot w_n)} \right|^2 \cdot L(Q) \\
&= \left| \sum_{n={\rm C,g}} f_n(Q) e^{2\pi i(1\cdot u_n + 0\cdot v_n)} \exp\left[-4\ln 2 \frac{(Q-2\pi/d_{10})^2}{(2\pi/D)^2}\right] \right|^2 \cdot L(Q) \\
&= \left| \left[ J_0(QR_{\rm t}) f_{\rm C}(Q) e^{2\pi i(0)} + 2n_{\rm IN} J_0(QR_{\rm A}) f_{\rm g}(Q) e^{2\pi i(0)} + 2n_{\rm OUT} f_{\rm g}(Q) \left( e^{2\pi i(1/3)} + e^{2\pi i(2/3)} \right) \cdot \frac{1}{2} \right] \cdot \exp\left[-4\ln 2 \frac{(Q-2\pi/d_{10})^2}{(2\pi/D)^2}\right] \right|^2 \cdot L(Q) \\
&= \left| \left[ J_0(QR_{\rm t}) f_{\rm C}(Q) + 2n_{\rm IN} J_0(QR_{\rm A}) f_{\rm g}(Q) - n_{\rm OUT} f_{\rm g}(Q) \right] \exp\left[-4\ln 2 \frac{(Q-2\pi/d_{10})^2}{(2\pi/D)^2}\right] \right|^2 \cdot L(Q), \qquad (1)
\end{aligned}
$$

where $f_{\rm C}$, $f_{\rm g}$, $(h,k,l)$, $(u_n, v_n, w_n)$, $J_0$, $d_{10}$ and $L(Q)$ are atomic scattering factor for carbon, atomic scattering factor for nitrogen or oxygen atom, index of diffraction, fractional coordinate of atoms, Bessel function, *10* reflection plane space of hexagonal lattice $\sqrt{3}a/2$ and Lorentz factor, respectively. Here, we assume that the carbon atoms and gas molecules in the site A are distributed in the cylinder with radius $R_{\rm t}$ and $R_{\rm A}$, respectively, and use the Gaussian function as approximation of the Laue function. By using the parameters presented below, we find $J_0(QR_{\rm t})f_{\rm C}(Q) < 0$ and $J_0(QR_{\rm A})f_{\rm g}(Q), f_{\rm g}(Q) > 0$ around the peak position of *10* reflection ($Q \approx 0.42$). Therefore, the decrease of $I/I_0$ is expected for the adsorption in the site A, while the increase for the site B[7,8]. Detailed analysis will be presented below.

First, we discuss the results of $O_2$ adsorption in AG-SWNTs. For non-adsorbed SWNTs, the XRD profile can be reproduced by assuming using parameters of $R_t = 0.70$ nm, $a = 1.75$ nm, $D = 10.0$ nm. Because no defect is expected in AG-SWNTs, we expect that gases cannot enter the inside of tube and are adsorbed only on the site B. In this case, that is $n_{\rm IN} = 0$, $a$ and $n_{\rm OUT}$ are uniquely determined from $I/I_0$ and $Q_{10}$ in Figs. 4(a) and 4(b); results are plotted in Figs. 4(c) and 4(d). $a$ and $n_{\rm OUT}$ almost linearly increase up to around $V \approx 70$ (cm$^3$(stp)/g): This value corresponds to $V_m$, implying that site B is monolayer-adsorption-site. In addition, Fig. 4(c) shows that the lattice expand as gases being adsorbed on the site B, like $HNO_3$ intercalation into SWNT bundles[21]. This is contrast to the theoretical prediction[22] and experimental results on $CH_4$, Xe, and Ne[23], which were not confirmed to adsorbed in the site B. The schematic structural model for fully adsorbed AG-SWNTs is shown in Fig. 5(a). The molar number of adsorbed gas per carbon atom $n$ for this structure is estimated as 0.04 from the above XRD analysis. The value of $n = 0.04$ corresponds to $V = 75$(cm$^3$(stp)/g) which shows good agreement with the value estimated by isotherm $V = V_m = 70$(cm$^3$(stp)/g).

Next, we discuss the results of HT-SWNTs. In the contrast to the analysis of AG-SWNTs, there are three parameters, $a$, $n_{\rm IN}$ and $n_{\rm OUT}$. If they are independent each other, they cannot be determined. However, we can expect $n \equiv n_{\rm IN} + n_{\rm OUT}$ follow the relation between $n$ and $V$ as shown in Fig. 4(d) with solid line, because the purity of the HT-SWNTs is expected to be almost the same to that of the AG-SWNTs. Therefore, these three parameters can be uniquely determined from $I/I_0$ and $Q_{10}$. Obtained results are shown in Figs. 4(c) and 4(e). In the x-ray diffraction profile calculation, we used 0.37 nm as $R_{\rm A}$, which is obtained by subtracting the van der Waals radius of carbon 0.17 nm and the radius of gas molecule along the minor axis 0.16 nm from radius of nanotube 0.70 nm. From these results, we find that gases are almost adsorbed on the site A until $V$ reaches 80 (cm$^3$(stp)/g), where $n_{\rm IN}$ is 0.04 molecules per carbon atom. Above $V \approx 80$ (cm$^3$(stp)/g), the additional adsorption takes place mostly at the site B, and then both the $n_{\rm IN}$ and $n_{\rm OUT}$ reaches 0.05. Therefore, each half of monolayer-adsorption-gas is adsorbed on the site A and B, which is consistent with the result of adsorption isotherm. The schematic structural model of adsorption process for HT-SWNTs is shown in Fig. 5(b). Though the volumes of monolayer-adsorption-gas of the site A and B are almost the same, gases are not adsorbed on the both sites simultaneously, but are adsorbed by turns. This tendency suggests that the site A is more stable for gas-adsorption than the site B. It is interesting to clarify whether the reason of this difference is due to the difference in the surface electronic structure originating from curvature of graphen sheet[24] or to the difference of potential originating from carbon atom configuration[25].

In all cases, each adsorption-available-site can be accept about 0.05 molecules per carbon atoms as monolayer adsorption, which corresponds to the stoi-

chiometory of $C_{20}N_2$ or $C_{20}O_2$. It is reasonable for the site B, because it can be explained by the molecular alignment that the gas-molecules closely align in a row in the site B as shown in Fig. 5. On the other hand, in the site A, two molecules are adsorbed per cross section of SWNTs as shown in Fig. 5(b). This concentration is rather dilute compared with large spatial area of the site A, which can accommodate more than four molecules as shown in Fig. 1. The present situation in the site A may be analogue to the two-chains alignment of iodine atoms in the iodine intercalated SWCNTs[26]. The reason of the dilute gas-adsorption into inside of SWCNTs is interesting to be solved.

## 4 SUMMARY AND CONCLUSIONS

We have systematically studied the $N_2$ and $O_2$ adsorption properties of SWNT bundles and their structures. We have found that the SWNT bundle is an adsorbent with the Langmuir-type adsorption isotherm and that gas-adsorption process depends on the treatment of SWNTs. In the case of AG-SWNTs, gases are adsorbed only in the interstitial channels of the SWNT bundles. On the other hand, for the SWNTs with defects by heat-treatment, gases are adsorbed mostly on the inside surface of nanotubes in the low adsorption volume range and then mostly in the interstitial channels of the SWNT bundles in the high adsorption volume range. These results suggest that the inside of nanotubes is more stable for gas adsorption than the outside.

**Acknowledgements**

The authors are grateful to Prof. Y. Murakami, Dr. T. Shibata and Dr. T. Watanuki for helpful suggestions and valuable discussions. This work was supported in part by the research project, "Materials Science and Microelectronics of Nanometer-Scale Materials" (RFTF96P00104) from the Japan Society for the Promotion of Science, Japan and a Grant-in Aid for Scientific Research on the Priority Area "Fullerenes and Nanotubes" from the Ministry of Education, Science, Sports and Culture of Japan. One of authors (A.F.) was supported by a Grant-in Aid for Encouragement of Young Scientists (12740202) from The Ministry of Education, Science, Sports and Culture of Japan.

## References


[1] S. Iijima, Nature (London) **354** (1991) 56.

[2] P.M. Ajayan, T.W. Ebbesen, T. Ichihashi, S. Iijima, K. Tanigaki, and H. Hiura, Nature (London) **362** (1993) 522.

[3] E. Dujardin, T.W. Ebbesen, H. Hiura, and K. Tanigaki, Science **265** (1994) 1850.

[4] A.C. Dillon, K.M. Jones, T.A. Bekkedahl, C.H. Kiang, D.S. Bethune, and M.J. Heben, Nature (London) **386** (1997) 377.

[5] G.E. Gadd, M. Blackford, S. Moricca, N. Webb, P.J. Evans, A.M. Smith, G. Jacobsen, S. Leung, A. Day, and Q. Hua, Science **277** (1997) 933.

[6] J. Yano, S. Yoshizaki, S. Inagaki, Y. Fukushima, and N. Wada, J. Low Temp. Phys. **110** (1998) 573.

[7] Y. Maniwa, Y. Kumazawa, Y. Saito, H. Tou, H. Kataura, H. Ishii, S. Suzuki, Y. Achiba, A. Fujiwara, and H. Suematsu, Jpn. J. Appl. Phys. **38** (1999) L668.

[8] Y. Maniwa, Y. Kumazawa, Y. Saito, H. Tou, H. Kataura, H. Ishii, S. Suzuki, Y. Achiba, A. Fujiwara, and H. Suematsu, Mol. Cryst. Liq. Cryst. **340** (2000) 671.

[9] S.C. Tsang, P.J.F. Harris, and M.L.H. Green, Nature (London) **362** (1993) 520.

[10] C. Journet, W.K. Maser, P. Bernier, A. Loiseau, M. Lamy de la Chapelle, S. Lefrant, P. Deniard, R. Lee, and J.E. Fischer, Nature (London) **388** (1997) 756.

[11] H. Kataura, Y. Kumazawa, Y. Maniwa, I. Umezu, S. Suzuki, Y. Ohtsuka, and Y. Achiba, Synth. Met. **103** (1999) 2555.

[12] T. Shibata, Doctoral Thesis, University of Tokyo, 1996.

[13] Y. Murakami, and H. Suematsu, Phys. Rev. B **54** (1996) 4146.

[14] T. Shibata, Y. Murakami, T. Watanuki, H. Suematsu, Surf. Sci. **405** (1998) 153.

[15] S. Brunauer, P.H. Emmett, and E. Teller, J. Am. Chem. Soc. **60** (1938) 309.

[16] A.L. McClellan, H.F. Harnsberger, J. Colloid Interface Sci. **23** (1967) 577.

[17] I. Stepanek, L.C. de Menorval, R. Edwards, P. Bernier, AIP Conference Proc. **486** (1999) 456.

[18] A. Tess, R. Lee, P. Nikolaev, H. Dai, P. Petit, J. Robert, C. Xu, Y.H. Lee, S.G. Kim, A.G. Rinder, D.T. Colbert, G.E. Scuseria, D. Tománek, J.E. Fischer, and R.E. Smally, Science **273** (1996) 483.

[19] J.E. Fischer, A. Claye, and R.S. Lee, Mol. Cryst. Liq. Cryst. **340** (2000) 737.

[20] E. Anglaret, S. Rols, and J.-L. Sauvajol, Phys. Rev. Lett. **81** (1998) 4780.

[21] O. Zhou, B. Gao, C. Bower, L. Fleming, and H. Shimoda, Mol. Cryst. Liq. Cryst. **340** (2000) 541.

[22] G. Stan, M.J. Bojan, S. Curtarolo, S.M. Gatica, and M.W. Cole, Phys. Rev. B **62** (2000) 2173.

[23] . S. Talapatra, A.Z. Zambano, S.E. Weber, and A.D. Migone, Phys. Rev. Lett. **85** (2000) 138.

[24] A. Hirsch, H. Mauser, T. Clark, in *Molecular Nanostructures*, edited by H. Kuzmany, J. Fink, M. Mehring, and S. Roth (World Scientific, Singapore, 1997) pp. 55-60.

[25] S. Okada, A. Oshiyama, S. Saito, Phys. Rev. B **62** (2000) 7634.

[26] X. Fan, E.C. Dickey, P.C. Eklund, K.A. Williams, L. Grigorian, R. Buczko, S.T. Pantelides, and S.J. Pennycook, Phys. Rev. Lett. **84** (2000) 4621.

Fig. 1. Cross section SWNT bundle and candidate of gas adsorption sites. Large circles and closed circles represent nanotubes and gas-molecules, respectively. $R_{\rm t}$, $R_{\rm A}$ and $a$ denotes the radius of nanotube, the distance between the site A and the center of nanotube and the lattice constant of two-dimensional hexagonal lattice of SWNT bundle. Dashed line shows a unit cell of the lattice.

Fig. 2. Adsorption isotherms of $N_2$ (square) and $O_2$ (circle) molecules on AG- (closed mark) and HT- (open mark) SWNTs at 77.3 K. $p_0$ is the saturation pressure at 77.3 K. The inset shows the low pressure region on an extended scale. Lines are guides to the eye.

Fig. 3. X-ray diffraction patterns of the *10* reflection of hexagonal lattice of SWNT bundles on $O_2$ adsorption to (a) AG- and (b) HT-SWNTs for several specific pressures. The patterns were taken by subtracting the background signals from the raw data. The raw data are shown in the insets.

Fig. 4. Adsorbed gas volume dependence of the (a) intensity and (b) position of the *10* reflection for $N_2$ (square) and $O_2$ (circle) adsorption to AG- (closed mark) and HT- (open mark) SWNTs. The intensity is normalized by value of no-adsorbed ones. (c) the lattice constant of SWNT bundle, (d) $n_{\rm OUT}$ for AG-SWNTs and (e) $n_{\rm IN}$ and $n_{\rm OUT}$ for HT-SWNTs, which account for experimental results in (a) and (b). Marks in (c) are same for that of (a) and (b). In (d) and (e), open and closed mark shows data for $n_{\rm IN}$ and $n_{\rm OUT}$ for $N_2$ (square) and $O_2$ (circle) adsorption, respectively. Solid line is the expected total adsorbed gas number. Dotted lines are guides to the eye.

Fig. 5. Schematic structural model for gas-adsorbed (a) AG- and (b) HT-SWNTs. Large circles and closed circles represent nanotubes and gas-molecules, respectively.

Table 1
Monolayer adsorption capacity $V_m$ and specific surface area $A_s$ per gross weight of sample obtained by BET method.

| adsorbent | adsorbate | $V_m(\mathrm{cm}^3/\mathrm{g})$ | $A_s(\mathrm{m}^2/\mathrm{g})$ |
|---|---|---|---|
| as-grown | $N_2$ | 55 | 240 |
| | $O_2$ | 70 | 255 |
| heat-treated | $N_2$ | 115 | 501 |
| | $O_2$ | 146 | 534 |

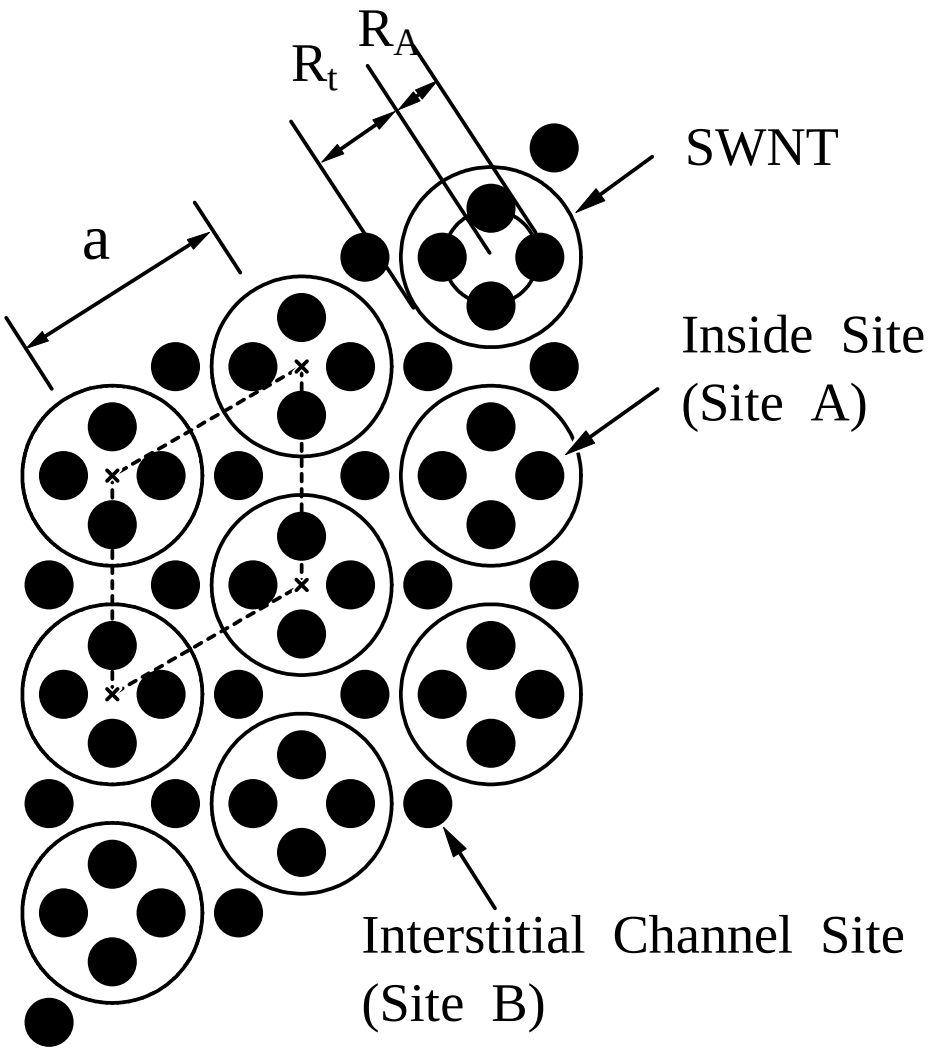


A. Fujiwara et al. Fig. 1

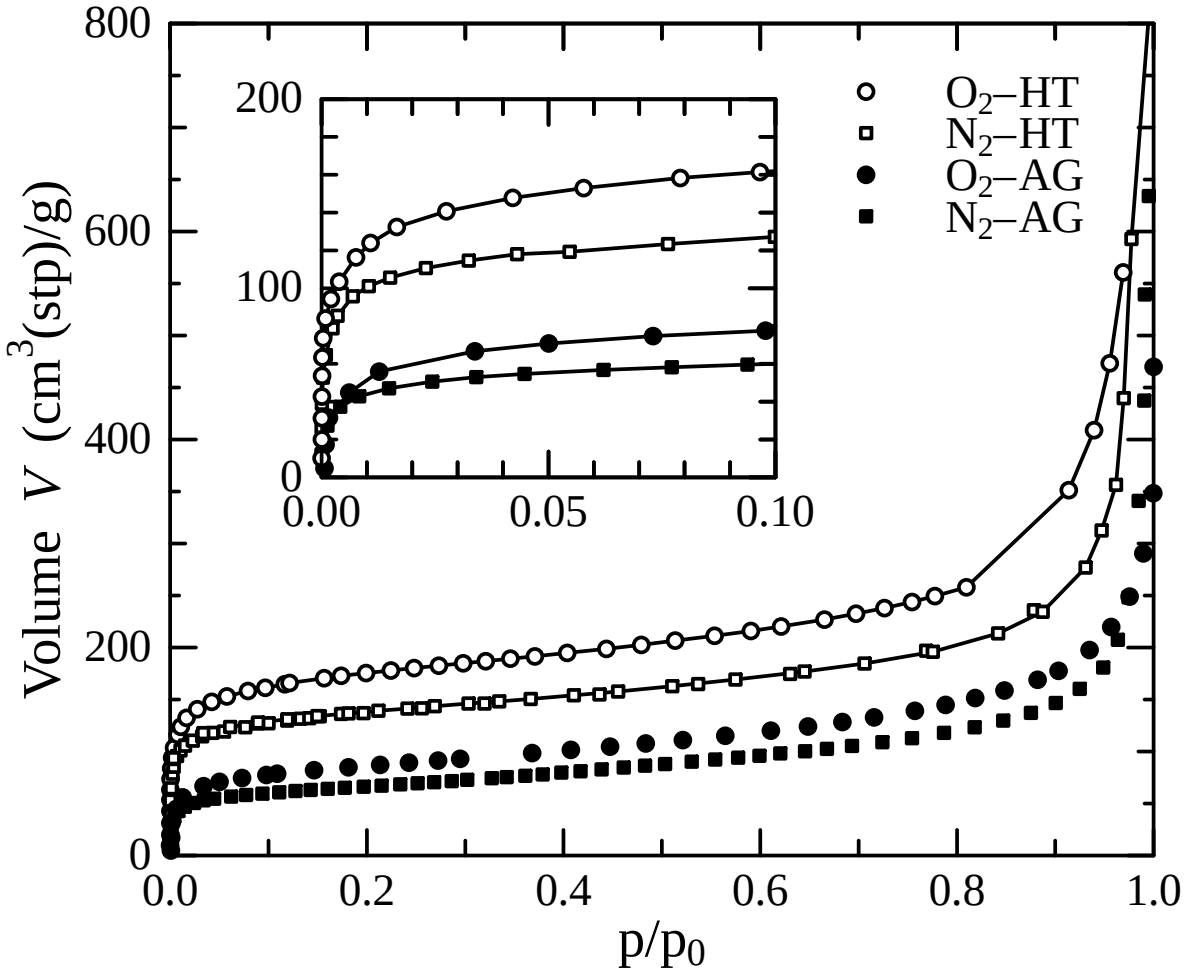


A. Fujiwara et al. Fig. 2

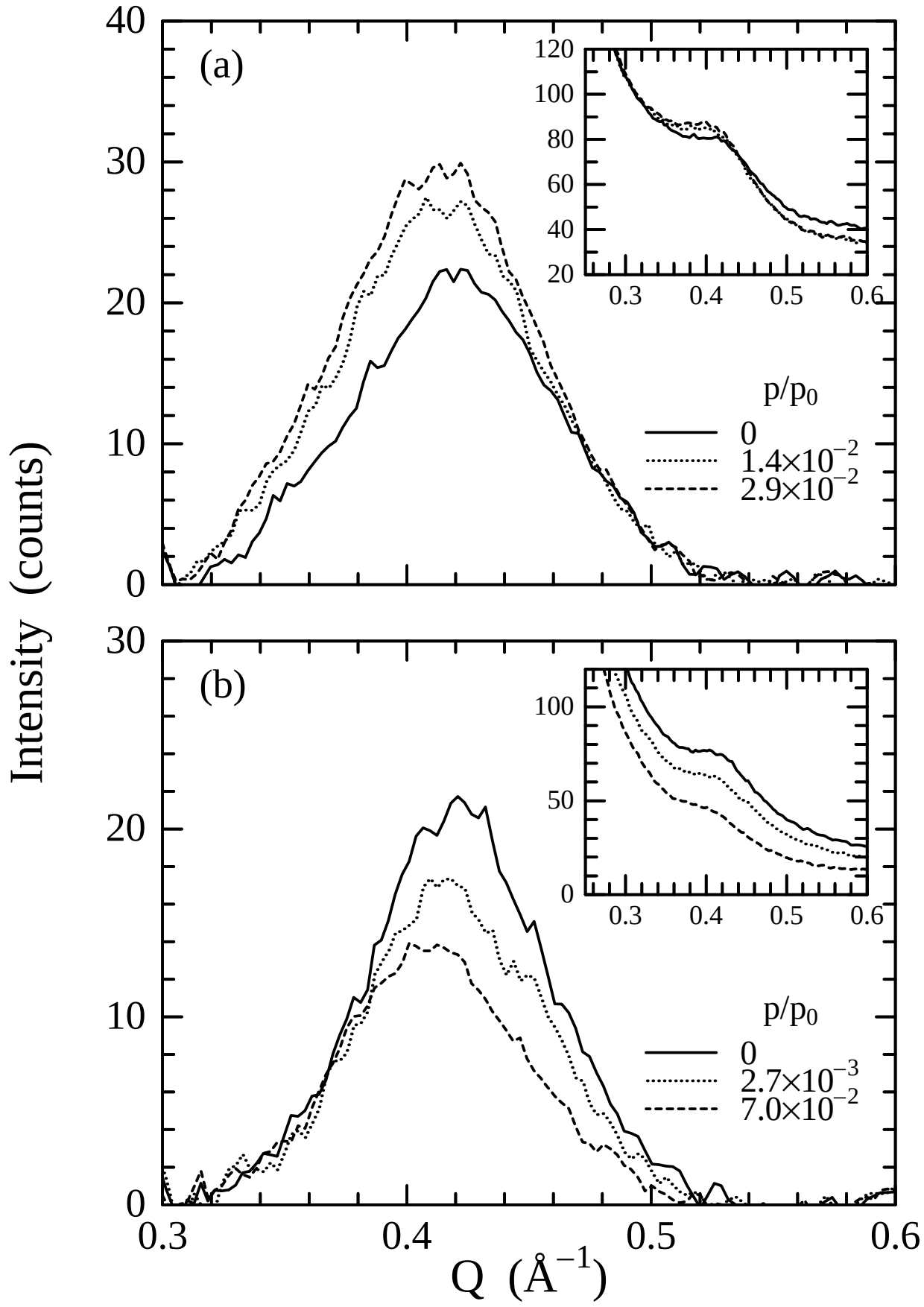


A. Fujiwara et al. Fig. 3

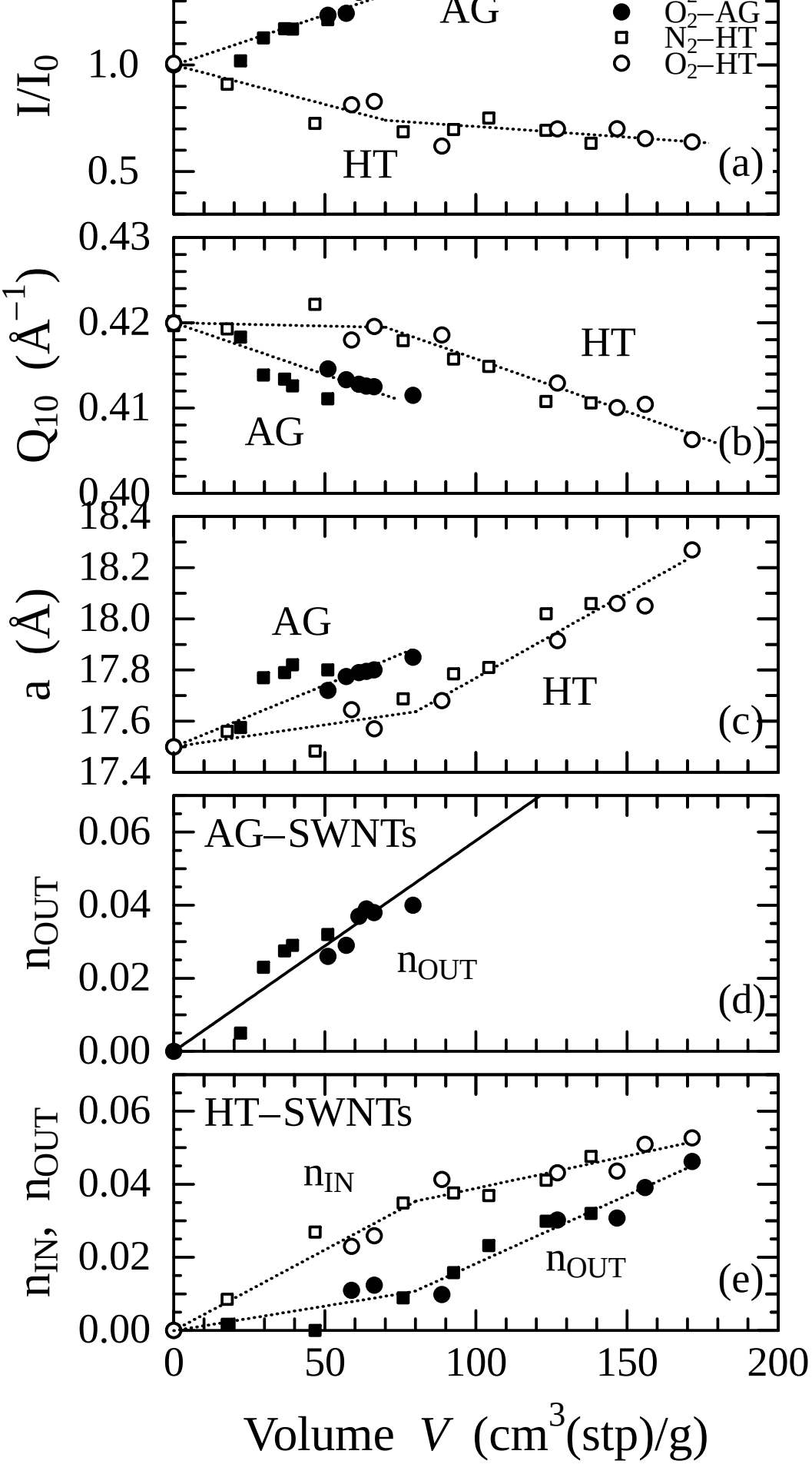


A. Fujiwara et al. Fig. 4

(a) AG–SWNTs

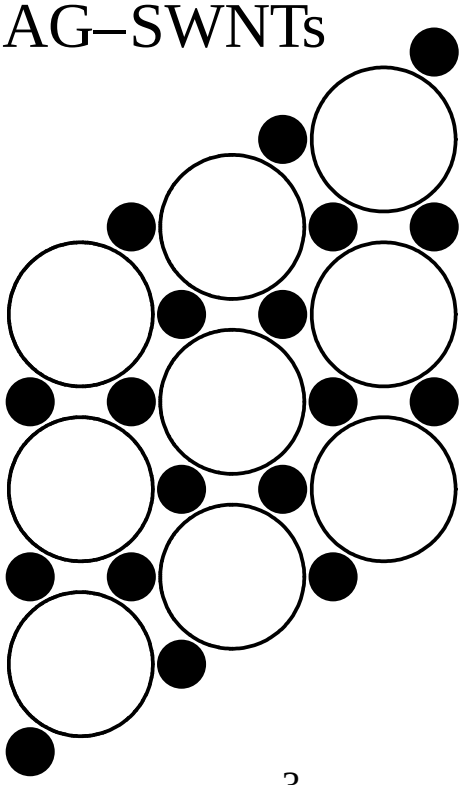

V ≈ 70 ($cm^3$(stp)/g)

(b) HT–SWNTs

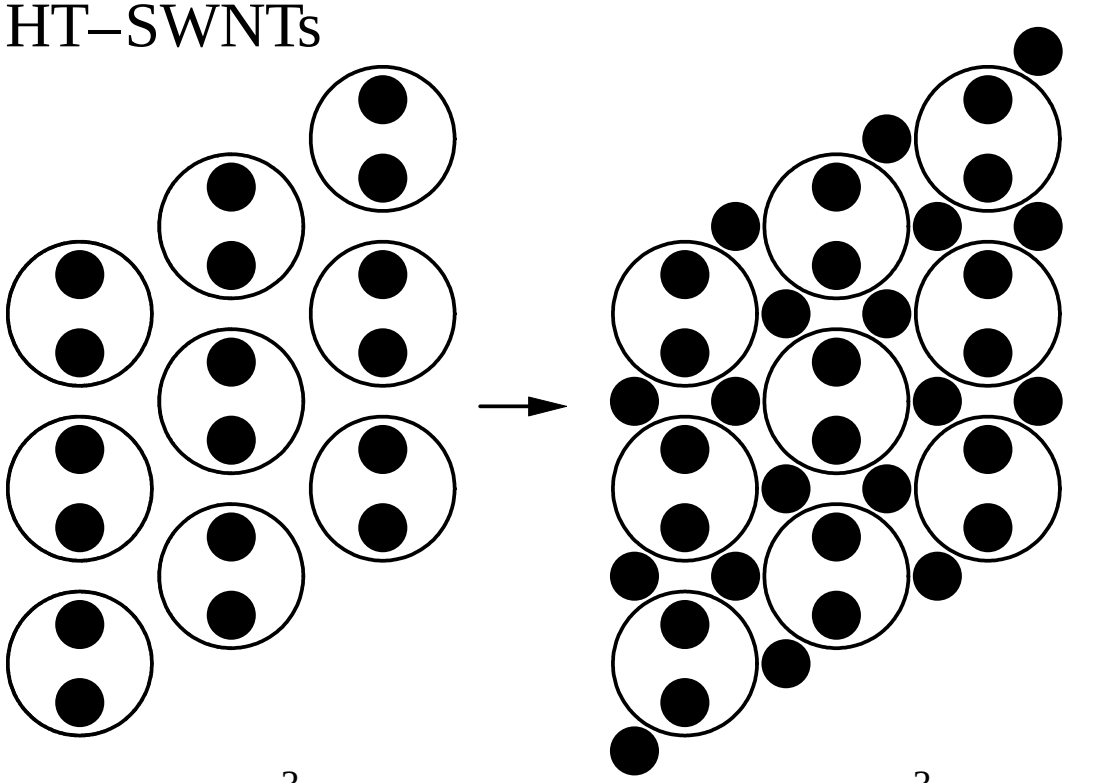

V ≈ 80 ($cm^3$(stp)/g)

V ≈ 170 ($cm^3$(stp)/g)

A. Fujiwara et al. Fig. 5